Available online at www.sciencedirect.com

ScienceDirect

Advances in Space Research 71 (2023) 80–96

ADVANCES IN SPACE RESEARCH
(a COSPAR publication)

www.elsevier.com/locate/asr

Long-lasting Electromagnetic Ion Cyclotron wave signatures at Indian Antarctic Station, Maitri

Amar Kakad *, Aditi Upadhyay, Bharati Kakad, Rahul Rawat

Indian Institute of Geomagnetism, New Panvel, Navi Mumbai 410218, India

Received 1 July 2022; accepted 7 August 2022
Available online 12 August 2022

Abstract

The long-lasting, persistence electromagnetic ion cyclotron (EMIC) waves can have a profound effect on the dynamics of the relativistic electrons in the Earth's radiation belt. EMIC waves observed on the ground are the manifestation of their generation in the Earth's inner magnetosphere. With the spacecraft measurements, it is difficult to determine their spatio-temporal extent and sustainability. In this context, in addition to the spacecraft observations the ground observations can give better insights into these features. We have identified the long-duration EMIC wave events observed at the subauroal station Maitri during 2011–2017. We have found a total of 12 EMIC wave events that are steadily observed for >10 h. The start times of these events are identified between 1.4–9.3 LT hours, and they lasted for 10–18 h. All these events are dominantly seen during the recovery phase of the weak-moderate geomagnetic storm. Comparison with spacecraft observations indicate the simultaneous EMIC waves in the magnetosphere within *L*–shell 4–6 with wider longitudinal coverage, and sufficiently long time presence in the magnetosphere. Simultaneous differential electron flux observations from Van Allen Probes indicate that approximately 90% of these EMIC waves were accompanied by a decrease in relativistic (2.6–4.2 MeV) electrons in the outer radiation belts.
© 2022 COSPAR. Published by Elsevier B.V. All rights reserved.

Keywords: EMIC wave occurrence; Inner magnetosphere; Pc1-Pc2 pulsations; Long-duration events; Radiation belts

1. Introduction

Numerous Earth-orbiting spacecraft have reported the observations of electromagnetic ion cyclotron waves in the Earth's magnetosphere(Anderson and Hamilton, 1993; Bräysy et al., 1998; Erlandson and Ukhorskiy, 2001; Engebretson et al., 2002; Usanova et al., 2008; Fraser et al., 2010; Halford et al., 2010; Pickett et al., 2010; Min et al., 2012; Sakaguchi et al., 2013; Zhang et al., 2014; Remya et al., 2015; Kim et al., 2016; Matsuda et al., 2018; Vines et al., 2019; Wang et al., 2019; Grison et al., 2021; Lee et al., 2021; Kim et al., 2021; Jun et al., 2021). In the inner magnetosphere, they are excited through the free energy from hot ion temperature (≈ 1–100 keV) anisotropy (Kennel and Petschek, 1966; Thorne and Horne, 1997; Omura et al., 2010) and emit power in separate frequency bands at the local ion gyrofrequencies, namely, the proton band between the H^+ and He^+ gyrofrequencies, the helium band between the He^+ and O^+ gyrofrequencies, and the oxygen band below the O^+ gyrofrequency(Saikin et al., 2015). The processes such as substorm injections (Blum et al., 2015; Remya et al., 2018), magnetospheric compressions (Anderson and Hamilton, 1993; Usanova et al., 2008; Jun et al., 2019), and the effects of Shabansky orbits (McCollough et al., 2012) are known to be responsible to create a population of hot anisotropic protons required to excite these waves. Spacecraft observations have shown that the EMIC waves are preferentially generated in the

* Corresponding author.
E-mail address: amar.kakad@iigm.res.in (A. Kakad).

https://doi.org/10.1016/j.asr.2022.08.021
0273-1177/© 2022 COSPAR. Published by Elsevier B.V. All rights reserved.

regions where the hot anisotropic ions of the ring current spatially overlap with the cold dense plasma populations of the outer plasmasphere, plasmapause (Zhang et al., 2014; Tetrick et al., 2017) and the "edges" of plasmaspheric plumes(Fraser and Nguyen, 2001; Usanova et al., 2013; Halford et al., 2015) indicating that the overlapping region is favourable for triggering the ion cyclotron instability. After their generation, these waves propagate along geomagnetic field lines to the mid- and high-latitude ionosphere. A part of EMIC wave energy can get trapped into the F-region ionospheric duct and propagate horizontally to lower or higher latitudes, which can be detected on the ground. As a result, a long history of ground observations has provided a solid scientific understanding of EMIC waves (Kakad et al., 2018; Mann et al., 2014; Engebretson et al., 2015; Kakad et al., 2019; Upadhyay et al., 2020; Upadhyay et al, 2022a; Upadhyay et al., 2022b).

The spacecraft observations and simulation studies have revealed that the EMIC waves play an important role in particle dynamics and regulate the Earth's inner magnetospheric dynamics in several ways. For example, they can (1) potentially cause loss of relativistic electrons from the outer radiation belt to the atmosphere through pitch angle scattering (Omura and Zhao, 2012; Kurita et al., 2018; Ni et al., 2015; Yuan et al., 2018; Lee et al., 2020; Capannolo et al., 2021), (2) interact with the ring current particles and scatter them to loss cone causing the ring current decay during the recovery phase of the magnetic storm (Thorne and Horne, 1994; Shreedevi et al., 2021; Yahnin et al., 2021), (3) heat the heavy ions through resonant wave-particle interaction (Anderson and Fuselier, 1994; Horne and Thorne, 1997; Ma et al., 2019). The spatial and temporal distributions of the EMIC waves are key factors that determine their impact on the particle dynamics both in the ring current and radiation belt regions. Therefore, understanding the spatial and temporal distributions of EMIC waves in the inner magnetosphere is crucial to assess their impacts. While these waves are often thought to be localized and of short durations, sometimes they persist for a long duration. The literature review shows that few single event-based studies have focused on the long duration EMIC waves (Mann et al., 2014; Paulson et al., 2014; Blum et al., 2020). Mann et al., 2014 have analyzed the event with continuous EMIC waves for about greater than 18 h observed by the Canadian array of induction coil magnetometers in North America. In conjunction with this ground observation, both Van Allen Probes A and B (65° magnetic longitude apart) observed EMIC waves in a very narrow L-shell region (ΔL∼0.1–0.4) with the duration of about ∼10–15 min. This event was further analyzed by Usanova et al., 2013 to investigate interactions between EMIC waves and ultrarelativistic electrons from both observational and modeling perspectives. Their study demonstrated that the EMIC waves trigger ultrarelativistic (∼2–8 MeV) electron loss, which is confined to pitch angles below 45°, and do not affect the core electron distribution.

Table 1
The characteristics of the EMIC wave events, namely, lower and upper frequencies (f_l and f_u), centered frequency, associated maximum power, start time, end time, event duration (Δt), frequency range ($\Delta f = f_u - f_l$) are provided in this table for 12 long duration events under study. In addition, the minimum *SYMH* on the preceding day of the events and τ, which represents the time lag between the occurrence of minimum *SYMH* and the start time of EMIC wave activity are given. In the last column, the observations related to variations in the interplanetary solar wind parameters, *AE*-index, and solar wind pressure during the EMIC wave activity period are stated.

Event No.	Day	f_l [Hz]	f_u [Hz]	f_c [Hz]	$Power_{max}$ $[nT^2/Hz]\times10^{-2}$	t_{start} [UT hrs]	t_{end} [UT hrs]	Δt [hrs]	Δf [Hz]	$SYMH_{min}$ [nT]	τ [hours]	Remarks
1	06/04/2012	0.2	0.85	0.44	7.26	3.78	19.75	15.97	0.65	−70	19.88	Recovery phase, no change in P/AE/Bz/Ey
2	12/04/2015	0.23	1.01	0.41	3.13	0.68	18.14	17.46	0.78	−88	15.18	Recovery phase, no change in P/AE/Bz/Ey
3	14/08/2015	0.14	0.68	0.33	6.78	3.5	21.15	17.65	0.54	−36	25.9	Recovery phase, no change in P/AE/Bz/Ey
4	01/08/2016	0.13	0.6	0.38	1.70	4.71	15.31	10.6	0.47	−42	80.86	Recovery phase, no change in P/AE/Bz/Ey
5	23/09/2016	0.16	0.71	0.51	3.74	5.25	17	11.75	0.55	−36	74.51	Recovery phase, no change in P/AE/Bz/Ey
6	03/04/2017	0.18	1.18	0.36	4.12	3.97	14.94	10.97	1	−84	156.9	Recovery phase, no change in P/AE/Bz/Ey
7	13/11/2017	0.4	1.42	0.66	4.47	2.6	13.4	10.8	1.02	−89	118.41	Recovery phase, no change in P/AE/Bz/Ey
8	10/04/2017	0.18	1.14	0.46	9.05	3.1	17.92	14.82	0.96	−36	25.18	Recovery phase, no change in P/AE/Bz/Ey
9	17/07/2013	0.18	1.25	0.47	3.83	8.6	19.1	10.5	1.07	−77	57.1	Recovery phase, no change in P/AE/Bz/Ey
10	21/08/2016	0.2	0.67	0.4	1.51	5.67	16.44	10.77	0.47	−32	69.38	Recovery phase, increase in P
11	21/04/2017	0.18	0.98	0.52	7.53	8.55	18.01	9.46	0.8	−45	28.3	Recovery phase, increase in P
12	02/08/2016	0.19	0.87	0.43	4.12	5.3	16.29	10.99	0.68	−42	105.45	Recovery phase, increase in P and AE

A study by Paulson et al., 2014 has also reported the EMIC wave event with the short time period in space, but simultaneous ground observations of this event imply long-duration wave activity. By combining both in situ and ground-based data, they found that the region satisfying electromagnetic ion cyclotron wave generation conditions is azimuthally large while radially narrow. Recently, Blum et al., 2020 reported the long duration EMIC wave event observed by Van Allen probes on 7 July 2013, which persisted for over 10 h and spanned the entire nightside of the Earth. They also reported local minima in electron phase space density, which is consistent with EMIC wave driven scattering and loss of MeV electrons from the outer radiation belt. It demonstrates that such persistent, extended EMIC waves have the potential to produce significant effects on the loss of energetic particle dynamics in the inner magnetosphere. Thus, examining such long duration EMIC wave events with ground and satellite observations is essential to advance our knowledge about their characteristics and generation source.

Although the above-mentioned studies of long-duration EMIC wave events have been reported, this problem is still insufficiently explored as all such studies were based on a single event. Encouraged by this, we explore the ICM data for the period of 2012 to 2017 at the Indian Antarctic station Maitri to investigate the long-duration EMIC wave events. The possible triggers for these long-duration EMIC wave events are also examined. We explore the possibility of the simultaneous signature of EMIC waves and the dynamics of the relativistic electron population in the inner magnetosphere by using observations from the Van Allen Probes. The remaining paper is organized as follows: we describe the data and the methodologies used for selecting the long-duration EMIC wave events in Section 2. The results are discussed in Section 3. In this section, the general characteristics of the long duration events are discussed in SubSection 3.1. The possible triggers for these long-duration events are examined in SubSection 3.2. The simultaneous signatures of EMIC waves in the outer radiation belt on these 12 event-days are discussed in 3.3. In SubSection 3.4, we have investigated the variation in relativistic electrons in the outer magnetosphere during these long-duration events. The present study is summarized and concluded in Section 4.

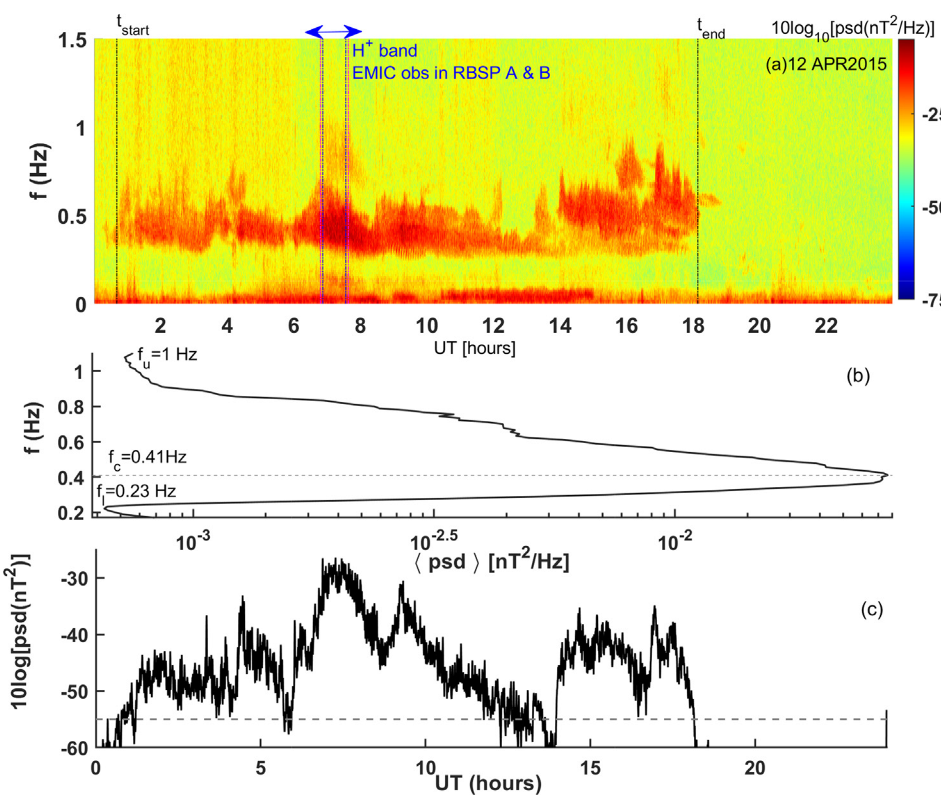

Fig. 1. (a) Shows spectrogram of the horizontal component of magnetic field variation recorded by ICM at Maitri on 12 April 2015. The resolution of the spectrogram is 0.011 Hz and 18 s. The start time (t_{start}) and end time (t_{end}) of the EMIC wave activity are shown with dashed-dotted lines. The time duration for which the EMIC wave activity observed by RBSP-A (magenta color) and RBSP-B (blue color) in the H^+ band is marked by dashed-dotted lines. (b) The EMIC wave power in the spectrogram is averaged in time from t_{start} to t_{end} and plotted as a function of frequency. The lower frequency f_l= 0.23 Hz, upper frequency f_u=1.01 Hz are marked. The centered frequency f_c=0.41 Hz, where the maximum power localized is shown by the horizontal dashed line. (c) The averaged spectrogram power from frequency f_l to f_u as a function of UT time. The level of −55 dB power is shown by the horizontal dashed line as a reference.

2. Data information

We have utilized ground Induction Coil Magnetometer (ICM) data recorded at the Indian Antarctic station, Maitri (geographic lat. 70.7^o S, geographic long. 11.8^o E, L∼5) from 2011 to 2017 to identify the long duration EMIC wave events. The sampling frequency of the data is either 64 Hz or 256 Hz. For each day, the Fourier spectrogram of the variation in the horizontal component of the magnetic field is obtained. The power spectral density in the spectrogram is estimated from $B(f,t) = P_x(f,t) + P_y(f,t)$. Here, $P_x(f,t), P_y(f,t)$ are the power spectral densities of individual magnetic field components B_x, and B_y, respectively. The resolution of the spectrogram is 0.011 Hz and 18 s. These spectrograms are carefully examined to identify the long duration EMIC wave events. In this study, a long duration event means the EMIC waves with sufficient power continuously seen in the spectrogram for approximately 10 h or more in the Pc1-Pc2 frequency range (0.1–5 Hz). This way, we could identify 12 such EMIC wave events during the specified period of seven years. These EMIC wave events are listed in Table 1, and they are termed as event-1, event-2 up to event-12. In order to understand the possible triggers for these long duration EMIC wave events, we have examined the interplanetary solar wind conditions at the magnetopause and geomagnetic activity indices like $SYMH$ and AE-index. The $SYMH$ index is the proxy to measure the strength of ring current during geomagnetic storms, and the AE-index is used to identify the substorm activity. In general, it is believed that the particle injection during substorm activity and solar wind pressure impulse are the possible sources to trigger the generation of EMIC waves in the Earth's magnetosphere (Remya et al., 2018, Upadhyay et al., 2022a). The interplanetary solar wind parameters like dynamic pressure (P), solar wind velocity (V_{sw}), interplanetary magnetic field Bz-component (IMF-Bz), interplanetary electric field Ey-component (dawn-to-dusk) are obtained from OMNIWeb (https://omniweb.gsfc.nasa.gov/), and the geomagnetic activity indices like $SYMH$ and AE are obtained from World Data Center (WDC) Kyoto (http://wdc.kugi.kyoto-u.ac.jp).

It may be noted that such long duration EMIC wave events with steady power in the Pc1-Pc2 range for a longer time are observed sparsely on the ground. After scrutiny of seven years of dataset, we could get only 12 events. We have examined the variation in relativistic electron flux and simultaneous EMIC wave signatures in the outer radi-

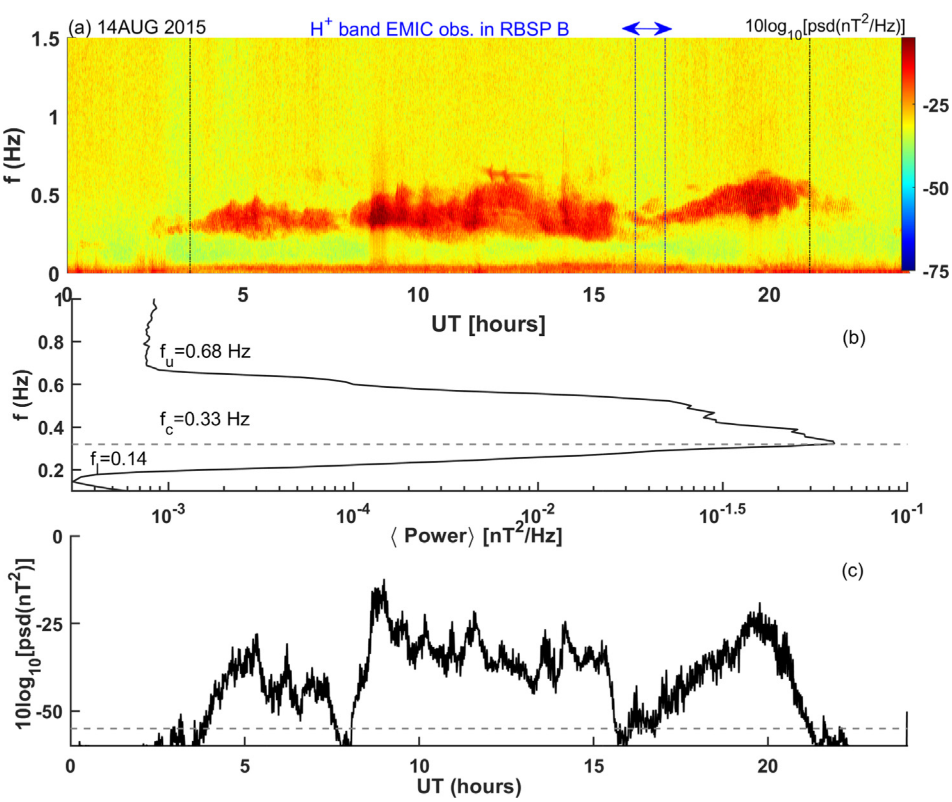

Fig. 2. (a) Shows the spectrogram of the horizontal component of magnetic field variation observed at Maitri on 14 August 2015. The start time (t_{start}) and end time (t_{end}) of the EMIC wave activity are shown with dashed-dotted lines. The time duration for which the EMIC wave activity observed by RBSP-B (blue color) in the H^+ band is marked by dashed-dotted lines. (b) The EMIC wave power in the spectrogram is averaged in time from t_{start} to t_{end} and plotted as a function of frequency. The lower frequency f_l= 0.14 Hz, upper frequency f_u=0.68 Hz are marked. The centered frequency f_c=0.33 Hz, where the maximum power is localized is shown by the horizontal dashed line. (c) The averaged spectrogram power from frequency f_l to f_u as a function of UT time. The level of −55 dB power is shown by the horizontal dashed line as a reference.

ation belt using dual-spacecraft Van Allen Probes A and B. The Van Allen Probes were earlier known as Radiation Belt Storm Probes (RBSP). The orbits of these spacecraft lie in the Earth's equatorial plane below the geosynchronous orbit in such a way that it spans L-shell in the range of 1.1–6.5. Here, we utilized the data from two instruments, namely, (i) Electric and Magnetic Field Instrument Suite and Integrated Science (EMFISIS) magnetometer instrument and (ii) Energetic Particle Composition and Thermal Plasma (ECT) suite. The EMFISIS magnetometer has a sensitivity of 0.01nT^2/Hz and it provides three components of ambient magnetic field sampled at 64 Hz (Kletzing et al., 2013). We utilized level-3 magnetic field data available at the SPDF OMNIWeb portal. In the ECT suite, there are different instruments (like HOPE, MagEIS, and REPT) and their details are provided in Boyd et al. (2019). The highest-energy instrument in the ECT suite is the REPT (Relativistic Electron Proton Telescope) and it provides the measurement of high-energy electrons in 12-energy channels ranging from 1.8–20 MeV (Baker et al., 2013b). The spin averaged differential electron flux level-2 data of 2-s resolution is obtained from the SPDF OMNIWeb portal and have been used in the present study. In next Section 3, we have discussed the results.

3. Results and discussion

3.1. General characteristics

In this section, we present the general characteristics of all 12 EMIC wave events that are considered in this study. For these events, sufficient power is observed continuously in the Pc1-Pc2 frequency range at Maitri. In Fig. 1, we present one illustrative example of long duration EMIC wave event observed at ground station Maitri on 12 April 2015 (event-2). Fig. 1(a) depicts the spectrogram of magnetic field variation for 24 h. The start (t_{start}) and end times (t_{end}) of this event are shown with dashed-dotted lines. On this day, both RBSP A and B have also observed EMIC

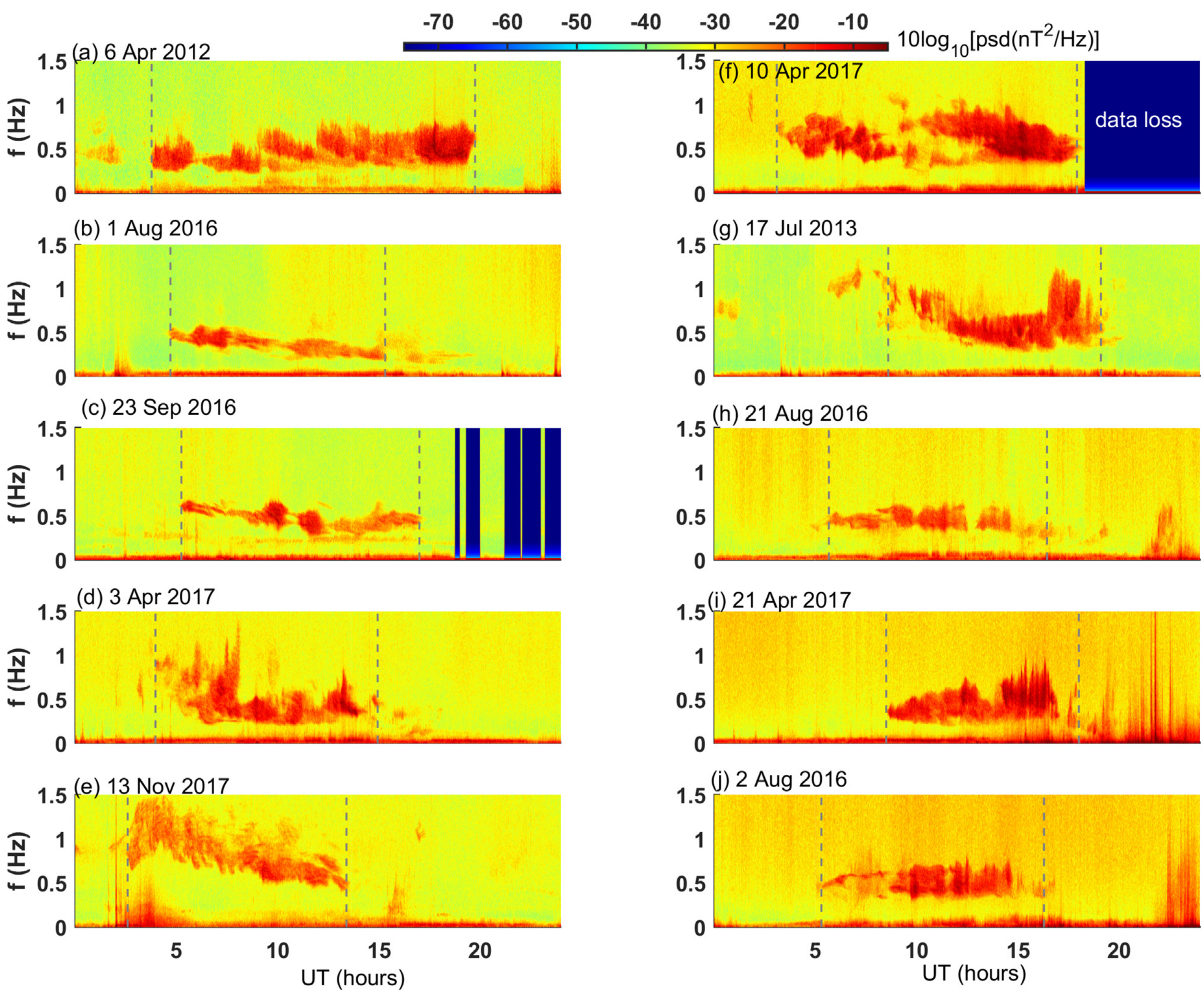

Fig. 3. (a-j) Shows spectrogram of the horizontal component of magnetic field variation observed at Maitri for events 1 and 4–12, respectively. The start time (t_{start}) and end time (t_{end}) of the EMIC wave activity for each of these events are shown with dashed-dotted lines. The data loss can be seen in deep blue color in panels (c) and (f).

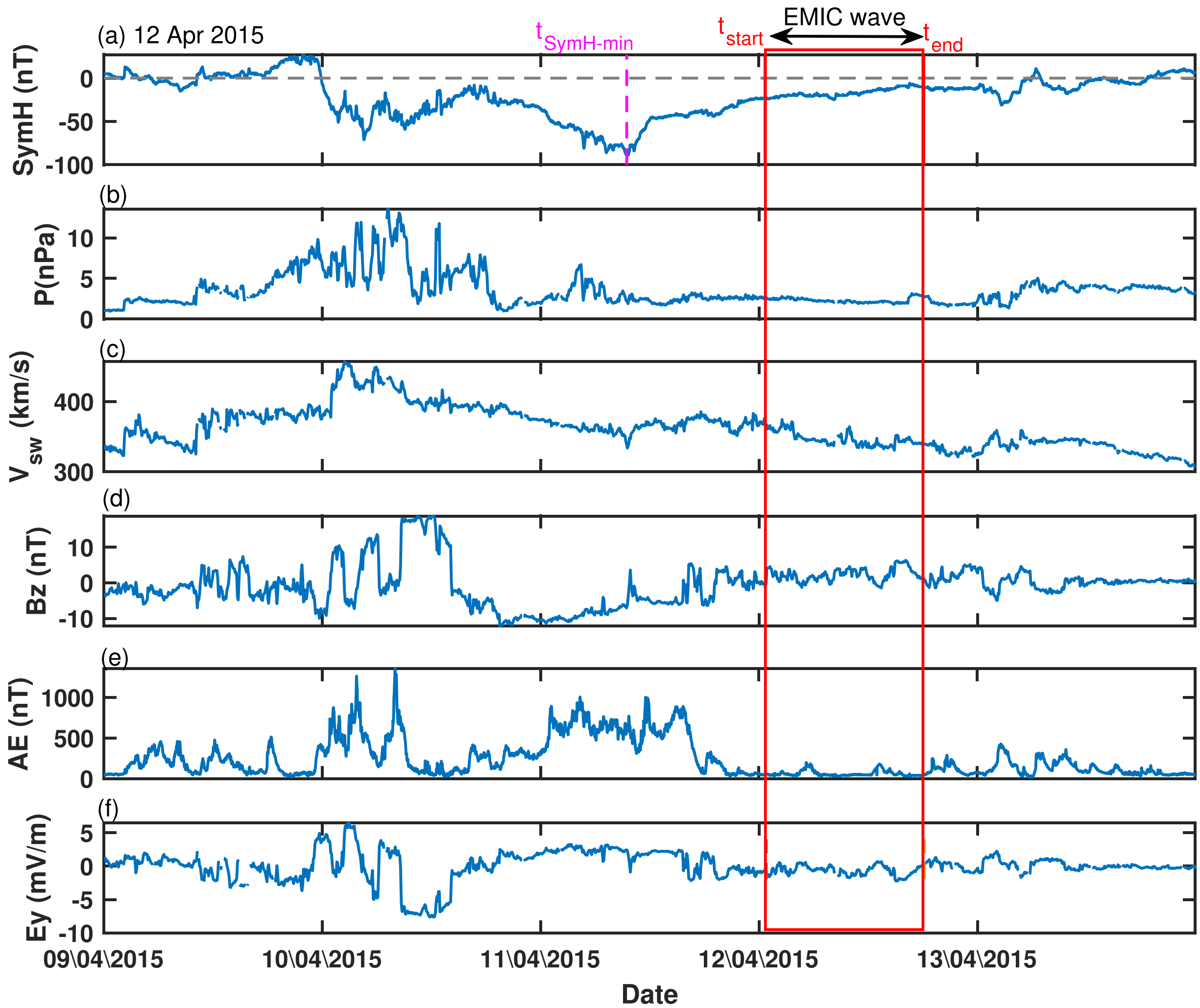

Fig. 4. (a-f) Shows the time variation of $SYMH$ (a proxy to measure ring current), solar wind pressure, solar wind speed, interplanetary magnetic field Bz-component (IMF-Bz), AE index and interplanetary electric field Ey component (IEF-Ey, i.e., dawn to dusk component) on 12 April 2015 (event-2). These parameters are shown from 9–13 April 2015 to visualize magnetospheric conditions on the preceding days of the event-2. The start and end times of the EMIC wave activity on 12 April 2015 are marked with red rectangles. The time of minimum in $SYMH$ is marked with magenta dashed line upper panel.

waves in the H^+ band. The duration of the EMIC waves observed by RBSP A and B are marked by magenta and blue dashed-dotted lines, respectively. The EMIC waves observed by RBSP A and B are discussed in later subsections. The EMIC wave power in the spectrogram is averaged in time from t_{start} to t_{end} and plotted as a function of frequency in Fig. 1(b). It can be seen that the EMIC wave has a frequency range of 0.23–1.01 Hz with maximum power around centered frequency, $f_c = 0.41$ Hz. The upper and lower frequencies associated with the EMIC wave are marked in Fig. 1(b), and the centered frequency is depicted by the dashed lines. Further, we have averaged spectrogram power from frequency f_l to f_u and it is plotted as a function of time in Fig. 1 (c). It is seen that the observed EMIC wave event has sufficient power, consistently from t_{start} to t_{end}, i.e. for about a duration of 17.5 h.

In Fig. 2 we have shown another long duration EMIC wave event observed on 14 August 2015 (event-3). This event is seen approximately from 3.5–21.15 UT hours with a duration of 17.6 h. As seen in Fig. 2b, the wave power for this event is centered around a frequency $f_c = 0.33$ Hz with an upper and lower frequency bound of 0.68 Hz and 0.14 Hz, respectively. On 14 August 2015, RBSP-B observed EMIC wave activity in the H^+ band. The duration of this event is marked by the blue vertical dashed-dotted lines in Fig. 2a. As mentioned earlier, overall, we have a total of 12 long duration EMIC wave events. For a clearer description of these events, we have labeled them as events 1–12. The spectrograms of the magnetic field variation for remaining events (i.e., event-1 and event 4–12) are shown in Fig. 3a-j, a-j, respectively. The details of these events viz. start time, end time, duration, frequency range, centered frequency, maximum power etc. are provided in Table 1. We noticed that the start times of these events are between 1.4–9.3 LT hours and they occurred for about 10–18 h. The centered frequencies corresponding to these

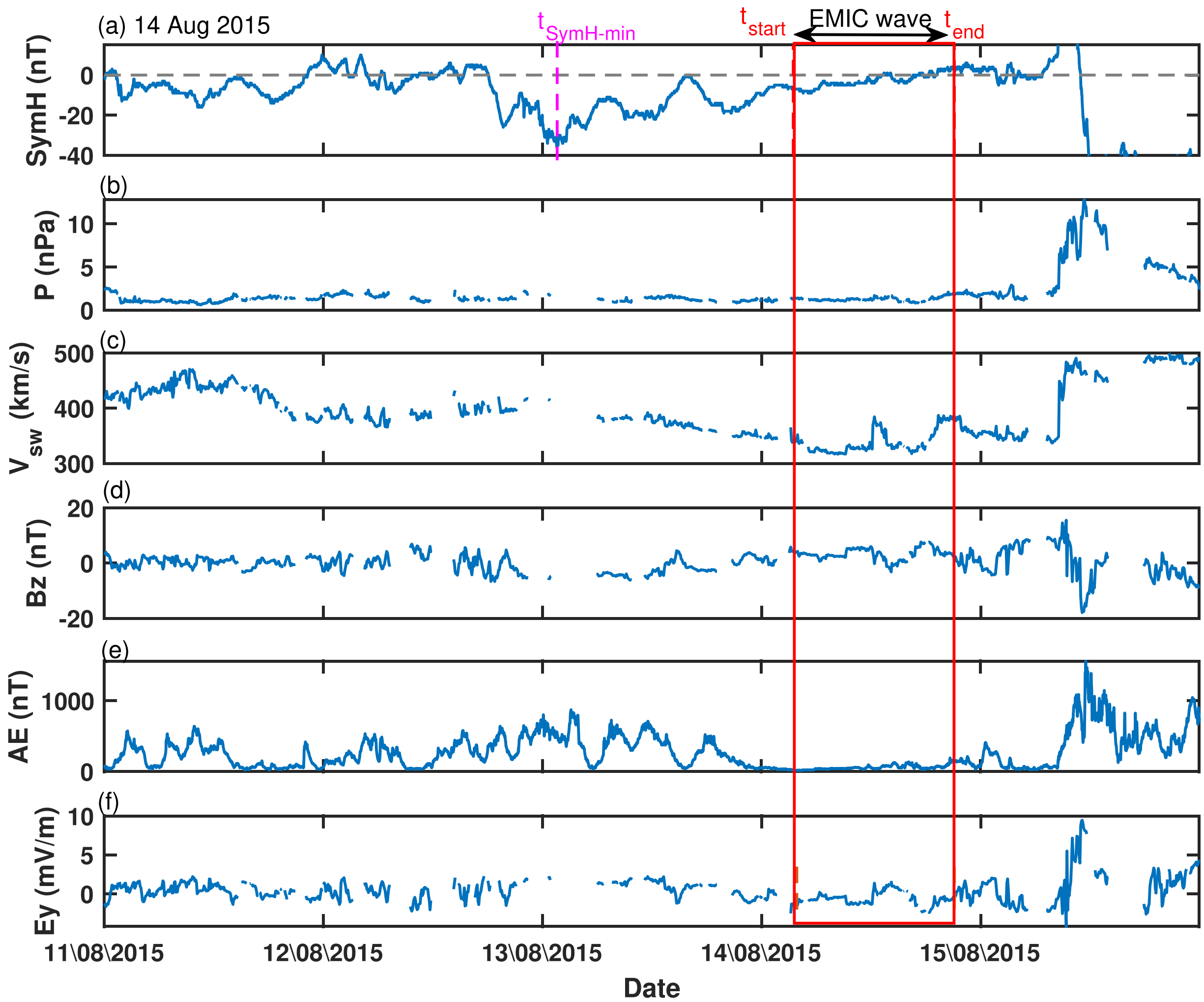

Fig. 5. (a-f) Shows the time variation of $SYMH$ (a proxy to measure of ring current), solar wind pressure, solar wind speed, interplanetary magnetic field Bz-component (IMF-Bz), AE index, and interplanetary electric field Ey component (IEF-Ey, i.e., dawn to dusk component) on 14 August 2015 (event-3). These parameters are shown from 11–17 August 2015 to visualize magnetospheric conditions on the preceding days of the event-3. The start and end time of the EMIC wave activity on 14 August 2015 is marked with a red rectangle. The time of minimum in $SYMH$ is marked with a magenta dashed line upper panel.

events vary between 0.33–0.66 Hz and their frequency extent (defined as $\Delta f = f_u - f_l$) varies in the range of 0.47–1 Hz. After exploring the general characteristics of EMIC waves, in the next subsection, we have looked into possible triggers for such long duration EMIC waves.

3.2. Possible triggers for long duration EMIC waves

In order to understand the possible triggers for these long duration EMIC waves we have examined the variation in interplanetary parameters like solar wind pressure (P), solar wind speed (V_{sw}), interplanetary magnetic field Bz–component (IMF-Bz), interplanetary electric field Ey–component (IEF-Ey), auroral activity index AE, and low latitude geomagnetic activity index $SYMH$ for the event days and their preceding days. The variation of $SYMH$, solar wind pressure, solar wind speed, IMF-Bz, AE index, and IEF-Ey (i.e., dawn to dusk component) are respectively shown in Fig. 4a-f for 12 April 2015 (event-2). These parameters are shown from 9–14 April 2015 to visualize magnetospheric conditions on the preceding days of the event-2. The start and end time of the EMIC wave activity observed on 12 April 2015 is marked with the red rectangle in Fig. 4. We can see that the long duration EMIC waves have occurred in the recovery phase of the moderate geomagnetic storm. The time of minimum in $SYMH$ is marked with the magenta dashed line in Fig. 4a. It may be noted that during the period of EMIC wave occurrence no drastic changes in the solar wind pressure, solar wind speed, IMF-Bz, AE and IEF-Ey are noticed. For 12 April 2015, the time lag $\tau = t_{start} - t_{symh-min}$ estimated to be 15.2 h. Furthermore, we have checked the interplanetary parameters and geomagnetic activity indices for EMIC wave activity observed on 14 August 2015 (event-3). The variation of $SYMH$, P, V_{sw}, IMF-Bz, AE index and IEF-Ey are respectively shown in Fig. 5a-f for 11–16 August 2015. The start

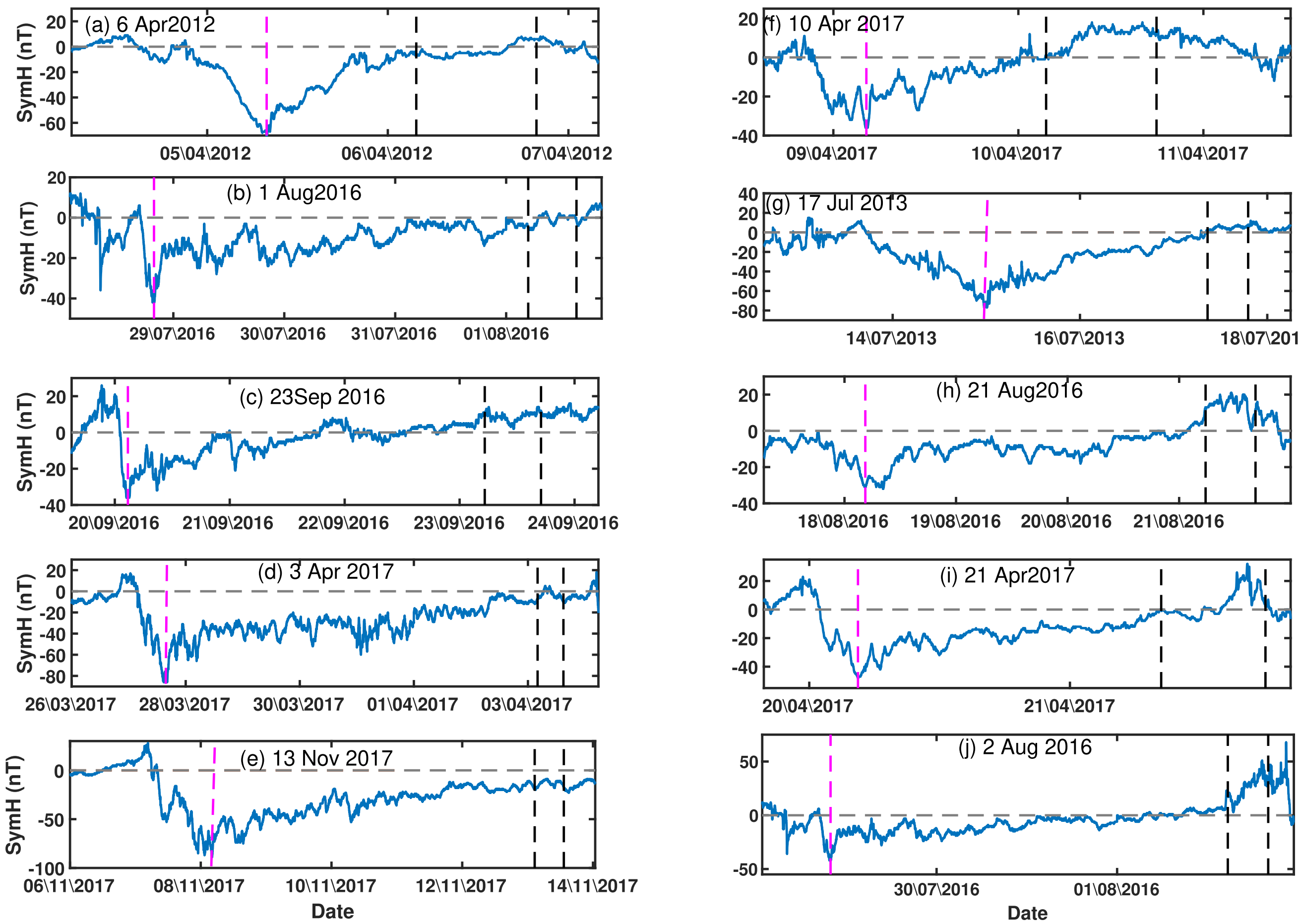

Fig. 6. (a-j) Shows the variation of $SYMH$ as a function of UT for events 1 and 4–12, respectively. The start and end time of the EMIC wave activity for each event is shown in respective panels by vertical dashed black lines. Also, the time of minimum in $SYMH$ for each event is marked with magenta in respective panels.

and end time of the EMIC wave activity observed on this day at Maitri is marked with the red rectangle in Fig. 5. It is evident from Fig. 5 that the observed long duration EMIC wave activity has also occurred in the recovery phase of the weak geomagnetic storm. The minimum in $SYMH$ and its time of occurrence ($t_{Symh-min}$) is shown with a magenta dashed line in Fig. 5a. The time lag (τ) between the time of occurrence of minimum in $SYMH$ and the start time of the EMIC wave is found to be 25.9 h for 14 August 2015.

In this way, we have carefully examined the interplanetary parameters and geomagnetic activity indices for other events as well (i.e., 1, and 4–12). For a better understanding and a clear visualization, we have plotted variation of $SYMH$ for events 1 and 4–12 in Fig. 6a-j, a-j, respectively. For all EMIC events, the minimum in $SYMH$, its time of occurrence, time lag τ and observations related to variation in interplanetary parameters during the time of occurrence of EMIC waves are summarized in Table 1. In this figure, the start and end time of the EMIC wave observed at Maitri for each event are marked with the vertical dashed lines. Similarly, the time of minimum in $SYMH$ prior to the start time of the EMIC wave activity for each event is marked with the magenta dashed line. We have noticed that all these long duration EMIC wave events are observed during the recovery phase of the weak-moderate geomagnetic storm. These events were preceded by either weak or moderate geomagnetic storm. Overall, for 9 events, no drastic change is observed in the interplanetary parameters and geomagnetic activity indices during the occurrence of the long duration EMIC wave activity. However, we have noticed an increase in solar wind pressure for event-10 (21 August 2016) and event-11 (21 April 2017), and an increase in both solar wind pressure and the AE index for event-12 (2 August 2016) during the occurrence time of EMIC wave activity. In Fig. 6 h-j, where $SYMH$ variation is respectively shown for event-10, event-11 and event 12, the rapid increase in $SYMH$ caused due to enhanced solar wind pressure is clearly visible. Although events 10–12 were preceded by the weak geomagnetic storm, the occurrence of EMIC waves on these days can not be attributed completely to the recovery phase of the geomagnetic storm. Thus, we conclude that out of 12 long duration EMIC wave events, 9 events (75% events) occurred clearly during

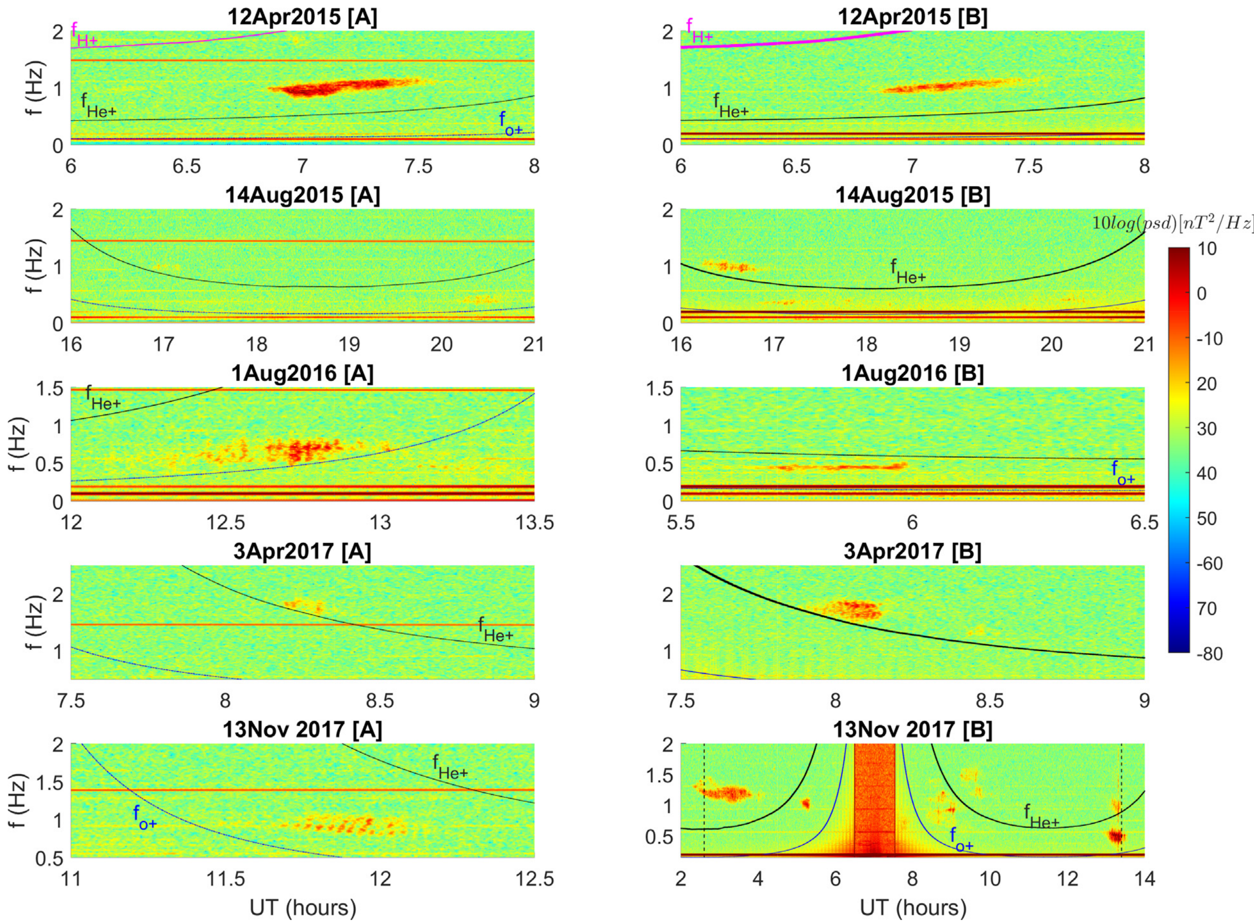

Fig. 7. Shows the spectrogram of magnetic field recorded by RBSP-A (left panels) and RBSP-B (right panels) for events 2–4 and 6–7, respectively starting from upper panel. The magenta, black and blue dashed-dotted lines respectively represent the local gyro frequencies of proton, helium and oxygen ions. Color bar represents power spectral density (PSD) of $B_{\perp}$ component.

the recovery phase of the weak-moderate geomagnetic storm. For 12 events, the $SYMH_{min}$ and time lag τ are provided in Table 1. The minimum $SYMH$ varies between -32 to -89 nT and the time lag between occurrence of minimum $SYMH$ and start time of EMIC wave is in the range of 15–156 h for events 1–12.

There are several studies using ground and spacecraft observations reporting the occurrence of EMIC waves during different phases of the geomagnetic storm. Using DE-1 satellite data Erlandson and Ukhorskiy (2001) reported that the EMIC wave occurrence rate enhances by a factor of five during the main and recovery phase of the geomagnetic storm as compared to a quiet day. In general, using satellite data, it is seen that the EMIC wave occurrence is also relatively higher during the main phase as compared to the recovery phase(Fraser et al., 2010). But on the ground, the EMIC wave observations indicate that they are generally not seen in the early phase of geomagnetic storm and it is more frequently observed during the late recovery phase (Engebretson et al., 2008a). It is attributed to the possible attenuation happening in the ionospheric heights (Kerttula et al., 2001). Obviously, in our study, we have not compared the occurrence of EMIC waves in different phases of the storm but we do notice that the long duration EMIC waves observed on the ground has a link to the recovery phase of the geomagnetic storm. The enhanced Pc1-Pc2 wave activity in 3–7 days following the storm main phase has been reported by other ground-based studies (Bortnik et al., 2008; Engebretson et al., 2008b). In all the above studies, the authors did not discuss the duration of EMIC waves. Here, the question is, "what could be the reason for the generation of such long duration EMIC wave activity in the late recovery phase of the geomagnetic storm?". Halford et al. (2010) have studied the occurrence of EMIC waves in different phases of the storm using CRRES satellite and found that in general, the occurrence rate of EMIC waves in the main phase is relatively higher as compared to the recovery phase (defined as 80% of minimum Sym-H value). These authors redefined the definition of the recovery phase and found that in the extended recovery phase (i.e., 4–6 days after the minimum in $SYMH$) the occurrence rate of EMIC waves was more. These authors proposed that the occurrences in the recovery phase of the storm could be associated with the expan-

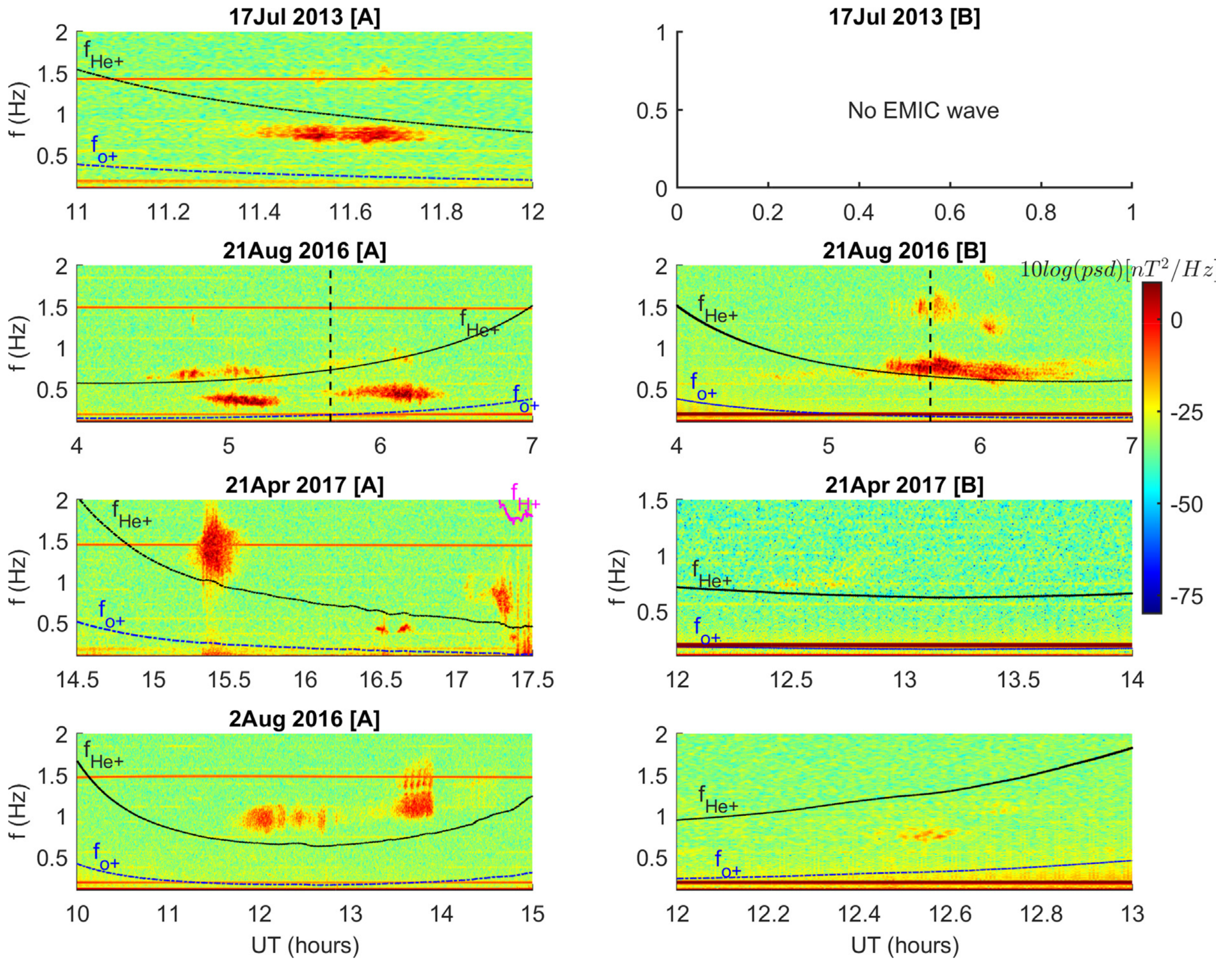

Fig. 8. Shows the spectrogram of magnetic field recorded by RBSP-A (leftside panels) and RBSP-B (rightside panels) for events 9–12 respectively starting from upper panel. The magenta, black and blue dashed-dotted lines respectively represent the local gyro frequencies of proton, helium and oxygen ions. Color bar represents power spectral density (PSD) of $B_\perp$ component.

sion of the plasmasphere as the storm has recovered. In our study, we found that the start time of these long-duration EMIC waves lies in the range of 1.4–9.3 LT hours (i.e., early morning sector). In a recent study, Wang et al. (2021) found that during the recovery phase of a storm the EMIC waves occur preferably in the 00–12 MLT sector. This shift in local time of EMIC wave occurrence is related to the eastward rotation of the plasmaspheric bulge toward morning during the late storm recovery phase and it overlaps with the ring current. It is in agreement with our study.

3.3. Simultaneous signature of the EMIC waves in space

The EMIC waves seen on the ground are the manifestation of EMIC waves generated in the inner magnetosphere. Thus, it is also important to understand the distribution of EMIC waves in the outer radiation belt on these 12 event-days. For this purpose, we used the EMFESIS magnetic field data from RBSP-A and B. We used two perpendicular components of the magnetic field sampled at 64 Hz to obtain the spectrogram of magnetic field variation. These magnetic field components are initially filtered in the 0.05–4 Hz frequency band and then used in the analysis. This is carried out using both RBSP-A and B observations. We checked these spectrograms for the simultaneous occurrence of EMIC waves in space for these 12 events. It should be noted that the event-1 is prior to the launch of Van Allen probes. Also, we have not observed any EMIC wave activity either in RBSP-A or RBSP-B for events 5 and 8. For the remaining events, the spectrograms of magnetic field recorded by RBSP-A and B are depicted in Figs. 7 and 8. The magenta, black and blue dashed-dotted lines respectively represent the local gyro frequencies of proton, helium and oxygen ions. The occurrence time of EMIC waves, their durations and associate stop bands (H^+ or He^+) are provided in Table 2. For the majority of events, we have observed the presence of EMIC waves either by RBSP A or RBSP B during the time period when long duration EMIC waves were observed at Maitri. The durations of EMIC waves observed by RBSP-A and B are in the range of 0.2-2 h. It may be noted that EMIC

Table 2
The decrease in the differential electron flux in the seven energy channels, namely, e1-e7 corresponding to 1.8–6.3 MeV observed by RBSP-A and RBSP-B on twelve long duration EMIC wave event-days is noted in the 3rd and 4th column of this table. Similarly, the details of EMIC wave activity, viz., durations and bands observed by RBSP-A and B are given in the last four columns.

Event	Day	Electron flux decrease	EMIC wave	RBSP-A		RBSP-B	
No.		Yes/No [Energies]	Yes/No [RBSP-A/B]	H+	He+	H+	He+
1	06/04/2012	Data not available	Data not available	—	—	—	—
2	12/04/2015	Yes [e1, e2, e3,e4,e5,e6]	Yes [RBSP-A and -B]	6.8–7.64	No	6.87–7.56	No
3	14/08/2015	Yes [e2, e3, e4,e5]	Yes [RBSP-B]	No	very faint	16.18–17.03	No
4	01/08/2016	Yes [e3, e4,e5]	Yes [RBSP-A and -B]	No	12.35–13.9	No	5.6–6
5	23/09/2016	Yes [e3, e4,e5]	No	No	No	No	No
6	03/04/2017	Yes [e4,e5,e6,e7]	Yes [RBSP-A and -B]	8.1–8.3	No	7.9–8.1	No
7	13/11/2017	Yes [e4,e5,e6,e7]	Yes [RBSP-A and -B]	11.63–12.14	No	2.1–4.1	5.1–5.4,8.5–9.2, 12.9–13.65
8	10/04/2017	Yes [e4,e5,e6]	No	No	No	No	No
9	17/07/2013	No	Yes [RBSP-A]	No	11.34–11.81	No	No
10	21/08/2016	Yes,[e3, e4, e4, e5]	Yes [RBSP-A and -B]	No	5.6–6.4	5.3–6.7	No
11	21/04/2017	Yes,[e3, e4,e5]	Yes [RBSP-A and -B]	17.2–17.4, 15.26–15.63	16.44–16.73	Very faint	No
12	02/08/2016	Yes [e3, e4]	Yes [RBSP-A and -B]	11.74–12.88, 13.43–13.96	No	No	12.47–12.63

wave duration as captured by spacecraft is governed by the trajectories of the satellite. If the satellite is not passing through the source region at the right time, it will miss the chance to detect that particular event. However, we are particularly exercising the long duration EMIC wave events and hence it is likely that we may find some simultaneous signatures of EMIC waves in space as well.

We have also examined the L-shell, latitude, longitude, and MLT spans during the time when EMIC waves are observed by RBSP-A and B. The average MLT, L-shell, longitude and latitude of the RBSP-A and B corresponding to the time of EMIC wave activity are shown in Fig. 9a-d, respectively. In this Figure, the red and blue colors represent the corresponding information from RBSP-A and B, respectively. It is clearly seen that all simultaneously observed EMIC waves are seen within L-shell span of 4–6. These EMIC waves had wider MLT coverage, which is expected because on the ground EMIC wave signatures were seen more than 10 h for all events considered here. The important feature is that the simultaneous occurrence of EMIC waves as detected in RBSP-A and B are mostly located 0–150 degree west from the longitude of Maitri (longitude of Maitri is marked with the dashed horizontal line in Fig. 9c). This indicates that the EMIC waves generated on these days had a wider longitudinal span and these waves persisted for a sufficiently long time to manifest their signatures in RBSP-A and B at the later time. It implies that when EMIC wave activity initiated in the inner magnetosphere ($L = 4 - 6$), their signatures were seen at Maitri at t_{start}, which continued with time as the source of EMIC wave was located in the wider longitudinal zone. At later time, when the RBSP spacecraft encountered the source region west side of Maitri, it could capture the EMIC wave activity. This confirms that the long duration EMIC waves had a wider longitudinal zone and they persisted for a sufficiently long time. A recent study by Blum et al. (2020) using multi-spacecraft observations reported the EMIC wave activity on 7 July 2013 that was limited to a narrow radial extent but persisting approximately more than 10 h and spanned 12 h in the local time. This event has also occurred in the recovery phase of the moderate geomagnetic storm with $SYMH_{min} \sim -80$nT. The simultaneous EMIC wave activity was also observed on the ground station Maitri for about 7.9 h, which is not shown here as it does not fall under the long duration events considered in the present study. Next, we have examined the outer radiation belt MeV range electron decrease during these long duration EMIC waves, which is discussed in the next subsection.

3.4. Observations of relativistic electrons by Van Allen probes

The EMIC waves can cause a rapid loss of high-energy electrons in the Earth's radiation belt (Usanova et al., 2014; Shprits et al., 2017; Kurita et al., 2018). These waves in the Earth's radiation belt can affect the loss process in all lon-

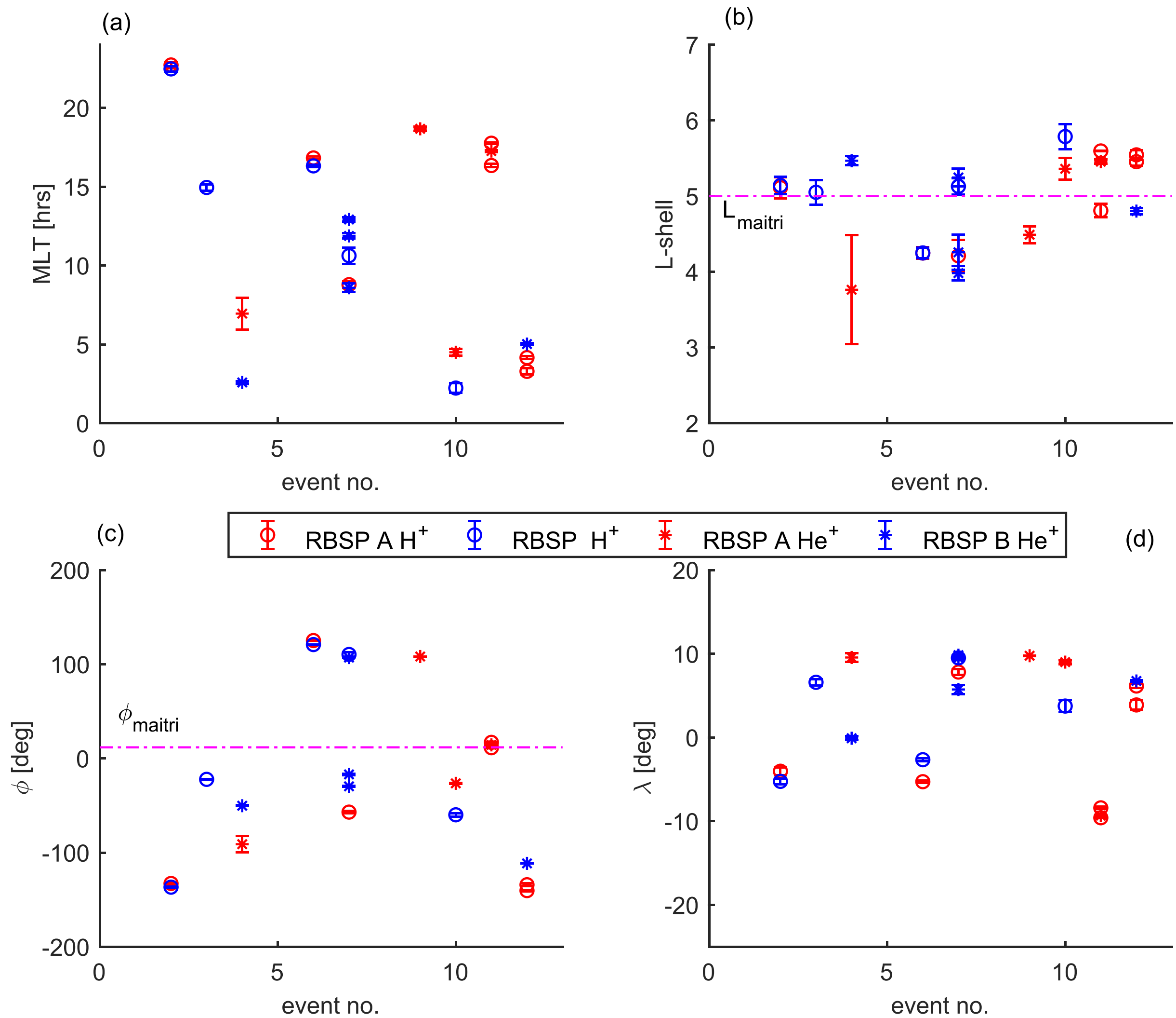

Fig. 9. The average (a) MLT, (b) L-shell, (c) longitude and (d) latitude for each single EMIC wave occurrence observed by RBSP-A and B either in H+ (shown by circle) or He + band (shown by asterisk) during the period of long duration EMIC wave events are shown with standard deviation as error bar for events 2–12. The L-shell and geographic longitude of Maitri is marked with dashed-dotted magenta lines in panel (b) and (c), respectively.

gitudes irrespective of their source location. This is because the MeV range electrons take few minutes to drift around the Earth in the outer radiation belt region. As a result, these electrons can interact with the EMIC waves present in any longitudinal zone several times, and eventually, they can get lost to the upper atmosphere. In order to understand the effect of the long duration EMIC waves on the MeV range electron flux, we have used the spin-averaged differential electron flux data from the REPT instruments aboard the Van Allen Probes. we have examined the electron flux in seven energy channels corresponding to (i)$e1$ =1.8 MeV, (ii)$e2$=2.1 MeV, (iii) $e3$ = 2.6 MeV, (iv)$e4$ =3.4 MeV (v)$e5$=4.2 MeV, (vi) $e6$ = 5.2 MeV, (iv)$e7$ =6.3 MeV. The remaining channels correspond to 7.7–20 MeV and are not considered in this study as the counts therein were low. Furthermore, we have not shown the relativistic electron observations for event-1 (6 April 2012), as this event observed on the ground is prior to the launch of RBSP.

In Fig. 10, we have shown the average differential electron flux as observed by RBSP-A and B as a function of time and L-shell for four energy channels $e2, e3, e4$, and $e5$. In this figure, panels (a-d) are for the day of event-2 (12 April 2015), whereas panels (e-h) show the flux observed on 26 April 2015, a geomagnetic quiet day on which no EMIC waves are seen. This quiet day is shown for the comparison purpose. The start time and end time of the EMIC waves observed on 12 April 2015 (event-2) at Maitri are marked by the white dashed-dotted lines. It is clearly evident from Fig. 10a-d that the electron flux in all four energy ranges (2.1–4.2 MeV) experienced a considerable decrease in the outer L-shells (L = 5–6) on the day of event-2. This noticeable decrease in electron flux is indicated with an arrow in Fig. 10a-d. Such a decrease in electron flux is not observed on the geomagnetic quiet day, 26 April 2015, with no EMIC wave activity (see Fig. 10e-h). In this way, we checked the electron flux variation for all events and the observations related to the decrease in elec-

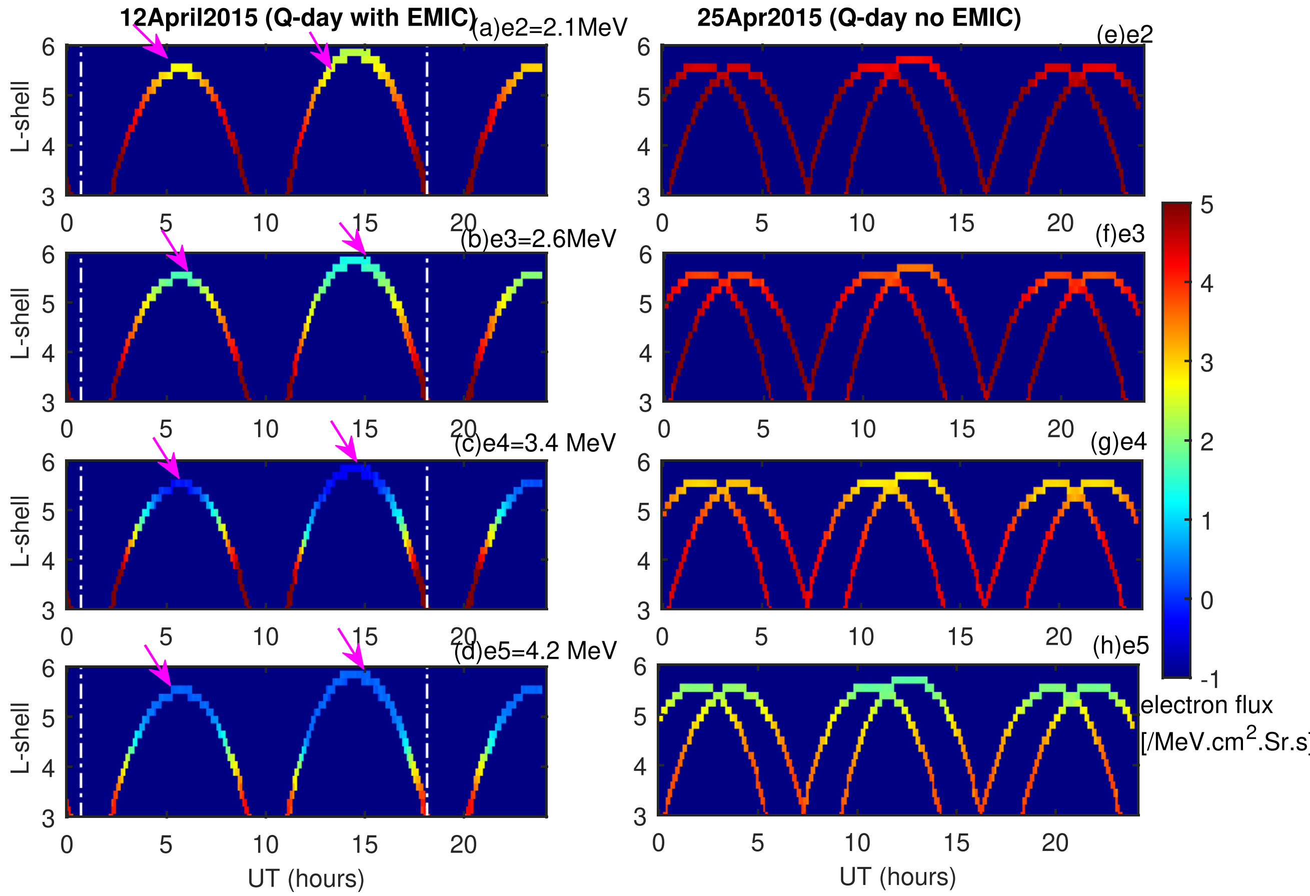

Fig. 10. (a-d) Shows average differential electron flux as observed by RBSP-A and RBSP-B as a function of time (UT) and L-shell for four energy channels *e*2, *e*3, *e*4, *e*5 for 12 April 2015 (event-2). Here, energy channels (i) *e*2=2.1 MeV, (ii) *e*3= 2.6 MeV, (iii) *e*4=3.4 MeV and (iv) *e*5=4.2 MeV. The differential electron flux is expressed in the units of $cm^{-2}s^{-1}sr^{-1}MeV^{-1}$. The start time and end time of the EMIC wave activity seen at Maitri are marked by the white dashed-dotted lines. Panels (e-h) are similar to (a-d) but they represents observations for a quiet day, 26 April 2015.

tron flux are documented in Table 2. The day corresponding to event-9 did not show any significant decrease in energies 1.8–6.3 MeV. Similar to Fig. 10, we plotted variation of electron flux for energy channels *e*2-*e*5 for events 3–7 in Fig. 11, and events 8–12 in Fig. 12. For all these long duration events noticeable decrease in MeV range electron flux is seen in the outer L-shells. Overall, we found that out of 11 events, 10 events (i.e., 90%) were associated with the decrease in 2.6–4.2 MeV electron flux during the occurrence of EMIC waves as seen at Maitri. Particularly, for events 6–8, the decrease in MeV range electron flux was found to be more in the higher energies (3.4–6.3 MeV). For these three events, the EMIC waves had a larger frequency extent($\Delta f > 1$ Hz) as compared to other EMIC wave events under study.

The energetic electron environment in the outer radiation belt is most dynamic and it is governed by various physical processes (like acceleration, transport, and loss) active therein at a given time (Turner et al., 2012; Baker et al., 2013a; Turner and Ukhorskiy, 2020). Due to such complexities, it is not straightforward to separate the dominant process responsible for the radiation belt electron flux variability. Many times these processes can cancel each other's effect and bring the electron flux in balance. The radiation belt dropout is the phenomenon where electron flux drops by several order in few hours. In general, the radiation belt higher energy electron dropouts can be attributed to two main mechanisms (i) magnetopause shadowing and (ii) scattering of electrons by EMIC waves (Medeiros et al., 2019). In the present study, events 10–12 are associated with increased solar wind pressure during the occurrence of EMIC waves and for remaining events, no drastic change is observed in interplanetary parameters. Thus, for events 10–12, the magnetopause shadowing process may have also contributed to the MeV range electron decrease. However, Xiang et al. (2017) reported that MeV range depletions at $L < 4$ is mainly associated with magnetopause shadowing, whereas at $L > 4$ it is associated with the EMIC waves. In our study, the electron decrease observed during the EMIC wave activity is mainly seen in the higher L-shells (i.e., $L = 4$–6). Thus, we can attribute it to the presence of long duration EMIC wave activity in the magnetosphere, whose signatures are manifested at ground station Maitri.

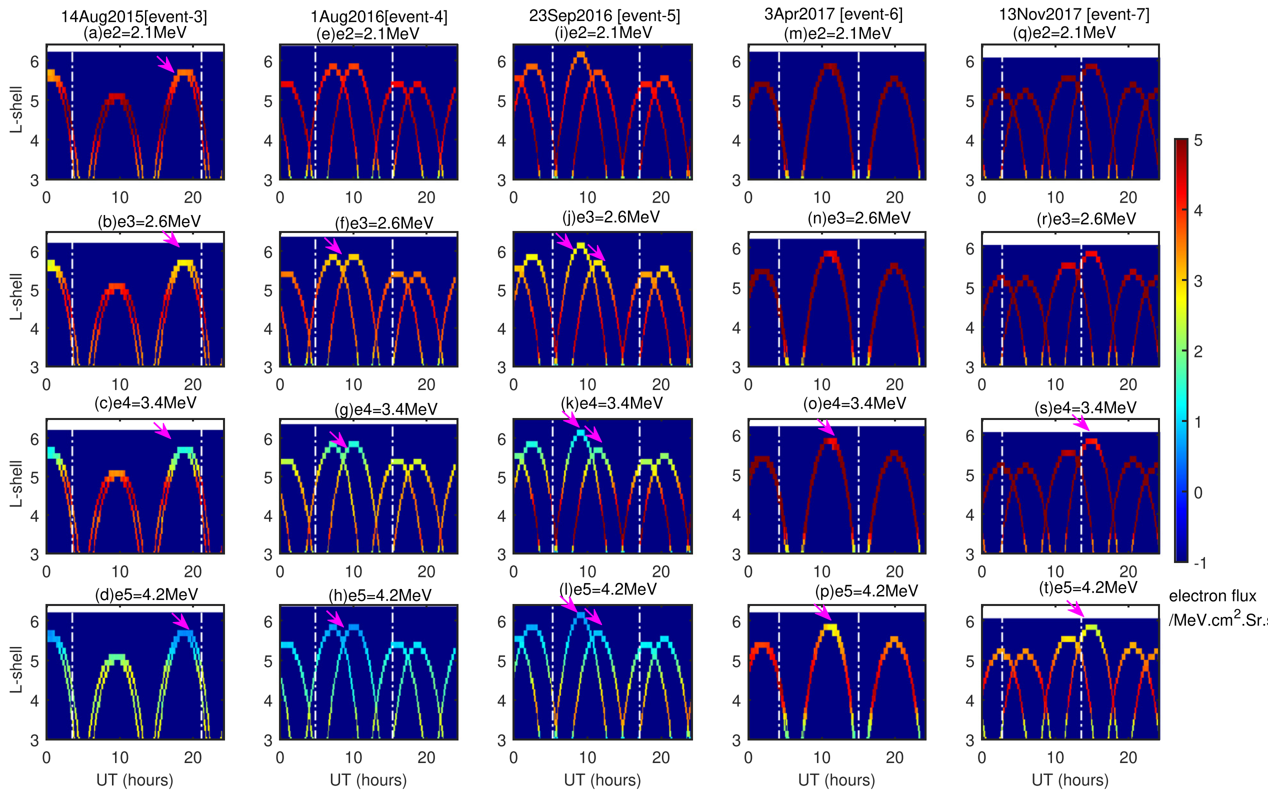

Fig. 11. Shows average differential electron flux as observed by RBSP-A and RBSP-B as a function of UT time and L-shell for four energy channels $e2$, $e3$, $e4$, $e5$ for events 3–7. Here, energy channels (i) $e2$=2.1 MeV, (ii) $e3$ = 2.6 MeV, (iii) $e4$ =3.4 MeV and (iv) $e5$ =4.2 MeV. The differential electron flux is expressed in the units of $cm^{-2}s^{-1}sr^{-1}MeV^{-1}$. The start time and end time of the EMIC waves seen at Maitri are marked by the white dashed-dotted lines. The considerable decrease in differential electron flux is marked with magenta arrows in each panel.

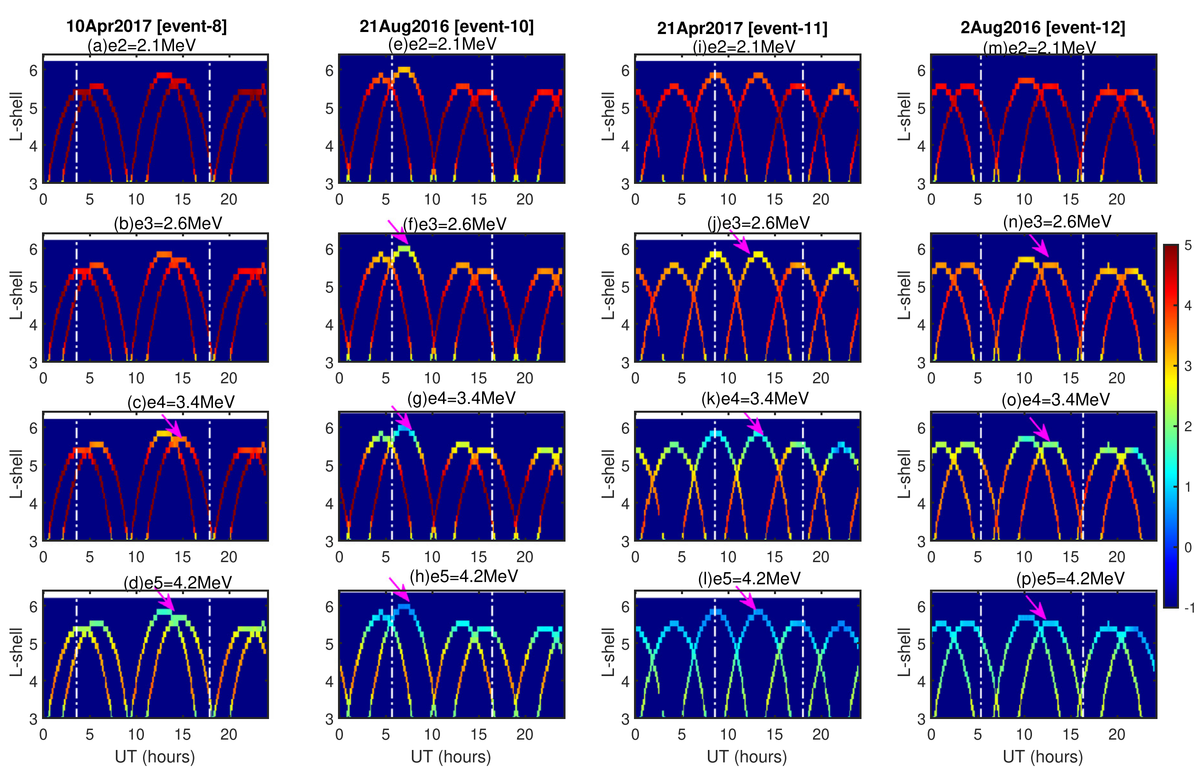

Fig. 12. Shows average differential electron flux as observed by RBSP-A and RBSP-B as a function of UT time and L-shell for four energy channels $e2$, $e3$, $e4$, $e5$ for event-8 and 10–12. Here, energy channels (i) $e2$=2.1 MeV, (ii) $e3$ = 2.6 MeV, (iii) $e4$ = 3.4 MeV and (iv) $e5$ = 4.2 MeV. The differential electron flux is expressed in the units of $cm^{-2}s^{-1}sr^{-1}MeV^{-1}$. The start time and end time of the EMIC waves seen at Maitri are marked by the white dashed-dotted lines. The considerable decrease in differential electron flux is marked with magenta arrows in each panel.

4. Summary and conclusions

In the present study, we have identified the long duration EMIC wave events observed at the Indian Antarctic station Maitri by examining the spectrograms of the magnetic field variations recorded by ICM during the period of 2011–2017. The location of this station is such that it falls in the subauroral zone with its L-shell (~5) close to the plasmapause location. Here, the long duration EMIC wave means the days when sufficient power in the Pc1-Pc2 frequency range is continuously detected for more than 10 h. The occurrence of such long duration EMIC wave events is less as we could get only 12 events over the period of seven years. Nevertheless, these long duration EMIC wave events can significantly affect the radiation belt dynamics. We have also used simultaneous particle and magnetic field data from RBSP satellites to get better insights about the relativistic electron decrease and the EMIC wave source location in the outer radiation belt. The characteristics of EMIC waves observed on the ground and by RBSP satellites are summarized in Table 1 and 2 along with corresponding remarks about the variations in interplanetary solar wind parameters, AE-index, and solar wind pressure. The main outcomes of the present study are listed below.

1. The long duration EMIC waves of duration 10–18 h as observed on the ground started in the post-midnight and early morning hours approximately 1.4–9.3 LT hours.
2. The centered frequency corresponding to these events is in the range of 0.33–0.66 Hz and their frequency extent defined as $\Delta f = f_u - f_l$ varies in the range of 0.47–1 Hz.
3. Most of the long duration EMIC wave events (~73%) occurred in the late recovery phase of the weak-moderate geomagnetic storm (-32 to −89 nT). It could be caused due to the expansion of the plasmasphere and the eastward rotation (i.e., toward the morning sector) of the plasmaspheric bulge during the late storm recovery phase (Halford et al., 2010; Wang et al., 2021).
4. The time lag (τ) between the occurrence of minimum $SYMH$ and the start time of EMIC wave activity at Maitri is in the range of 15–156 h with an average τ to be 65±45 h (~2.7 days).
5. Simultaneous EMIC wave occurrence in the inner magnetosphere was noticed in the L-shell~4–6. These long-duration EMIC waves were persistent and had a wider longitudinal extent.
6. These long-duration EMIC waves were accompanied by a decrease in 2.6–4.2 MeV electrons in the outer radiation belts. Furthermore, it is noticed that for the EMIC waves with a larger frequency extent ($\Delta f > 1$ Hz), the decrease in MeV range electron flux shifted towards the higher energies 3.4–6.3 MeV.

To conclude, apart from the characteristics of the long-duration EMIC waves, the present study using simultaneous ground and spacecraft observations of EMIC waves provides information about the possible longitudinal extent of the EMIC wave source region and its persistence in the outer radiation belt (L = 4–6). The present study clearly indicates that during the recovery phase of the weak-moderate geomagnetic storm, the conditions for the generation of EMIC waves are favorable in the wider longitudinal zone in the inner magnetosphere, which causes EMIC wave generation and their persistence for the longer time. Overall, the combination of ground-based and space-based data can be used efficiently to determine the spatio-temporal extent of the EMIC waves in the Earth's inner magnetosphere.

Declaration of Competing Interest

The authors declare that they have no known competing financial interests or personal relationships that could have appeared to influence the work reported in this paper.

Acknowledgments

We thank the OMNIWEB team for solar wind data available at http://omniweb.gsfc.nasa.gov and the WDC Kyoto for $SYMH$ and AE indices available at http://wdc.kugi.kyoto-u.ac.jp/. The EMIC data from Maitri is available at https://doi.org/10.5281/zenodo.5140227. We thank the polar team, IIG for ICM data. We acknowledge the Van Allen Probes data from the EMFISIS magnetometer instrument and ECT/REPT high energy particle data. Both these data are available at https://cdaweb.gsfc.nasa.gov.

References

Anderson, B., Hamilton, D.C., 1993. Electromagnetic ion cyclotron waves stimulated by modest magnetospheric compressions. J. Geophys. Res.: Space Phys. 98 (A7), 11369–11382. https://doi.org/10.1029/93JA00605.

Anderson, B.J., Fuselier, S.A., 1994. Response of thermal ions to electromagnetic ion cyclotron waves. J. Geophys. Res.: Space Phys. 99 (A10), 19413–19425. https://doi.org/10.1029/94JA01235.

Baker, D., Kanekal, S., Hoxie, V., et al., 2013a. A long-lived relativistic electron storage ring embedded in earth's outer van allen belt. Science 340 (6129), 186–190. https://doi.org/10.1126/science.1233518.

Baker, D.N., Kanekal, S., Hoxie, V., et al., 2013b. The relativistic electron-proton telescope (rept) instrument on board the radiation belt storm probes (rbsp) spacecraft: Characterization of earth's radiation belt high-energy particle populations. Space Sci. Rev. 179 (1–4), 337–381. https://doi.org/10.1007/s11214-012-9950-9.

Blum, L., Halford, A., Millan, R., et al., 2015. Observations of coincident emic wave activity and duskside energetic electron precipitation on 18–19 january 2013. Geophys. Res. Lett. 42 (14), 5727–5735. https://doi.org/10.1002/2015GL065245.

Blum, L.W., Remya, B., Denton, M.H., et al., 2020. Persistent emic wave activity across the nightside inner magnetosphere. Geophys. Res. Lett. 47 (6). https://doi.org/10.1029/2020GL087009, e2020GL087009.

Bortnik, J., Cutler, J., Dunson, C., et al., 2008. Characteristics of low-latitude pc1 pulsations during geomagnetic storms. J. Geophys. Res.: Space Phys. 113 (A4). https://doi.org/10.1029/2007JA012867.

Boyd, A., Reeves, G., Spence, H., et al., 2019. Rbsp-ect combined spin-averaged electron flux data product. J. Geophys. Res.: Space Phys. 124 (11), 9124–9136. https://doi.org/10.1029/2019JA026733.

Bräysy, T., Mursula, K., Marklund, G., 1998. Ion cyclotron waves during a great magnetic storm observed by freja double-probe electric field instrument. J. Geophys. Res.: Space Phys. 103 (A3), 4145–4155. https://doi.org/10.1029/97JA02820.

Capannolo, L., Li, W., Spence, H., et al., 2021. Energetic electron precipitation observed by firebird-ii potentially driven by emic waves: Location, extent, and energy range from a multievent analysis. Geophys. Res. Lett. 48 (5). https://doi.org/10.1029/2020GL091564, e2020GL091564.

Engebretson, M., Lessard, M., Bortnik, J., et al., 2008a. Pc1–pc2 waves and energetic particle precipitation during and after magnetic storms: Superposed epoch analysis and case studies. J. Geophys. Res.: Space Phys. 113 (A1). https://doi.org/10.1029/2007JA012362.

Engebretson, M., Peterson, W., Posch, J., et al., 2002. Observations of two types of pc 1–2 pulsations in the outer dayside magnetosphere. J. Geophys. Res.: Space Phys. 107 (A12), SMP-20. https://doi.org/10.1029/2001JA000198.

Engebretson, M., Posch, J., Westerman, A., et al., 2008b. Temporal and spatial characteristics of pc1 waves observed by st5. J. Geophys. Res.: Space Phys. 113 (A7). https://doi.org/10.1029/2008JA013145.

Engebretson, M.J., Posch, J.L., Wygant, J.R., et al., 2015. Van allen probes, noaa, goes, and ground observations of an intense emic wave event extending over 12 h in magnetic local time. J. Geophys. Res.: Space Phys. 120 (7), 5465–5488. https://doi.org/10.1002/2015JA021227.

Erlandson, R., Ukhorskiy, A., 2001. Observations of electromagnetic ion cyclotron waves during geomagnetic storms: Wave occurrence and pitch angle scattering. J. Geophys. Res.: Space Phys. 106 (A3), 3883–3895. https://doi.org/10.1029/2000JA000083.

Fraser, B., Grew, R., Morley, S., et al., 2010. Storm time observations of electromagnetic ion cyclotron waves at geosynchronous orbit: Goes results. J. Geophys. Res.: Space Phys. 115 (A5). https://doi.org/10.1029/2009JA014516.

Fraser, B., Nguyen, T., 2001. Is the plasmapause a preferred source region of electromagnetic ion cyclotron waves in the magnetosphere? J. Atmos. Solar Terr. Phys. 63 (11), 1225–1247. https://doi.org/10.1016/S1364-6826(00)00225-X.

Grison, B., Santolík, O., Lukačevič, J., et al., 2021. Occurrence of emic waves in the magnetosphere according to their distance to the magnetopause. Geophys. Res. Lett. 48 (3). https://doi.org/10.1029/2020GL090921, e2020GL090921.

Halford, A., Fraser, B., Morley, S., 2010. Emic wave activity during geomagnetic storm and nonstorm periods: Crres results. J. Geophys. Res.: Space Phys. 115 (A12). https://doi.org/10.1029/2010JA015716.

Halford, A.J., Fraser, B.J., Morley, S.K., 2015. Emic waves and plasmaspheric and plume density: Crres results. J. Geophys. Res.: Space Phys. 120 (3), 1974–1992. https://doi.org/10.1002/2014JA020338.

Horne, R.B., Thorne, R.M., 1997. Wave heating of he+ by electromagnetic ion cyclotron waves in the magnetosphere: Heating near the h+-he+ bi-ion resonance frequency. J. Geophys. Res.: Space Phys. 102 (A6), 11457–11471. https://doi.org/10.1029/97JA00749.

Jun, C.-W., Miyoshi, Y., Kurita, S., et al., 2021. The characteristics of emic waves in the magnetosphere based on the van allen probes and arase observations. J. Geophys. Res.: Space Phys. 126 (6). https://doi.org/10.1029/2020JA029001, e2020JA029001.

Jun, C.-W., Yue, C., Bortnik, J., et al., 2019. A statistical study of emic waves associated with and without energetic particle injection from the magnetotail. J. Geophys. Res.: Space Phys. 124 (1), 433–450. https://doi.org/10.1029/2018JA025886.

Kakad, A., Kakad, B., Omura, Y., et al., 2019. Modulation of electromagnetic ion cyclotron waves by pc5 ulf waves and energetic ring current ions. J. Geophys. Res.: Space Phys. 124 (3), 1992–2009. https://doi.org/10.1029/2017JA024930.

Kakad, B., Omura, Y., Kakad, A., et al., 2018. Characteristics of subpacket structures in ground emic wave observations. J. Geophys. Res.: Space Phys. 123 (10), 8358–8376. https://doi.org/10.1029/2018JA025473.

Kennel, C.F., Petschek, H., 1966. Limit on stably trapped particle fluxes. J. Geophys. Res. 71 (1), 1–28. https://doi.org/10.1029/JZ071i001p00001.

Kerttula, R., Mursula, K., Pikkarainen, T., et al., 2001. Storm-time pc1 activity at high and middle latitudes. J. Geophys. Res.: Space Phys. 106 (A4), 6213–6227. https://doi.org/10.1029/2000JA900125.

Kim, G.-J., Kim, K.-H., Lee, D.-H., et al., 2016. Occurrence of emic waves and plasmaspheric plasmas derived from themis observations in the outer magnetosphere: Revisit. J. Geophys. Res.: Space Phys. 121 (10), 9443–9458. https://doi.org/10.1002/2016JA023108.

Kim, H., Shiokawa, K., Park, J., et al., 2021. Statistical analysis of pc1 wave ducting deduced from swarm satellites. J. Geophys. Res.: Space Phys. 126 (3). https://doi.org/10.1029/2020JA029016, e2020JA029016.

Kletzing, C., Kurth, W., Acuna, M., et al., 2013. The electric and magnetic field instrument suite and integrated science (emfisis) on rbsp. Space Sci. Rev. 179 (1–4), 127–181. https://doi.org/10.1007/s11214-013-9993-6.

Kurita, S., Miyoshi, Y., Shiokawa, K., et al., 2018. Rapid loss of relativistic electrons by emic waves in the outer radiation belt observed by arase, van allen probes, and the pwing ground stations. Geophys. Res. Lett. 45 (23), 12720–12729. https://doi.org/10.1029/2018GL080262.

Lee, D.-Y., Kim, K.-C., Choi, C.-R., 2020. Nonlinear scattering of 90^o pitch angle electrons in the outer radiation belt by large-amplitude emic waves. Geophys. Res. Lett. 47 (4). https://doi.org/10.1029/2019GL086738, e2019GL086738.

Lee, J.H., Turner, D.L., Vines, S.K., et al., 2021. Application of cold and hot plasma composition measurements to investigate impacts on dusk-side electromagnetic ion cyclotron waves. J. Geophys. Res.: Space Phys. 126 (1). https://doi.org/10.1029/2020JA028650, e2020JA028650.

Ma, Q., Li, W., Yue, C., et al., 2019. Ion heating by electromagnetic ion cyclotron waves and magnetosonic waves in the earth's inner magnetosphere. Geophys. Res. Lett. 46 (12), 6258–6267. https://doi.org/10.1029/2019GL083513.

Mann, I.R., Usanova, M.E., Murphy, K., et al., 2014. Spatial localization and ducting of emic waves: Van allen probes and ground-based observations. Geophys. Res. Lett. 41 (3), 785–792. https://doi.org/10.1002/2013GL058581.

Matsuda, S., Kasahara, Y., Miyoshi, Y., et al., 2018. Spatial distribution of fine-structured and unstructured emic waves observed by the arase satellite. Geophys. Res. Lett. 45 (21), 11–530. https://doi.org/10.1029/2018GL080109.

McCollough, J., Elkington, S., Baker, D., 2012. The role of shabansky orbits in compression-related electromagnetic ion cyclotron wave growth. J. Geophys. Res.: Space Phys. 117 (A1). https://doi.org/10.1029/2011JA016948.

Medeiros, C., Souza, V., Vieira, L., et al., 2019. On the contribution of emic waves to the reconfiguration of the relativistic electron butterfly pitch angle distribution shape on 2014 september 12—a case study. Astrophys J 872 (1), 36. https://doi.org/10.3847/1538-4357/aaf970.

Min, K., Lee, J., Keika, K., et al., 2012. Global distribution of emic waves derived from themis observations. J. Geophys. Res.: Space Phys. 117 (A5). https://doi.org/10.1029/2012JA017515.

Ni, B., Cao, X., Zou, Z., et al., 2015. Resonant scattering of outer zone relativistic electrons by multiband emic waves and resultant electron loss time scales. J. Geophys. Res.: Space Phys. 120 (9), 7357–7373. https://doi.org/10.1002/2015JA021466.

Omura, Y., Pickett, J., Grison, B., et al., 2010. Theory and observation of electromagnetic ion cyclotron triggered emissions in the magnetosphere. J. Geophys. Res.: Space Phys. 115 (A7). https://doi.org/10.1029/2010JA015300.

Omura, Y., Zhao, Q., 2012. Nonlinear pitch angle scattering of relativistic electrons by emic waves in the inner magnetosphere. J. Geophys. Res.: Space Phys. 117 (A8). https://doi.org/10.1029/2012JA017943.

Paulson, K.W., Smith, C.W., Lessard, M.R., et al., 2014. In situ observations of pc1 pearl pulsations by the van allen probes. Geophys. Res. Lett. 41 (6), 1823–1829. https://doi.org/10.1002/2013GL059187.

Pickett, J., Grison, B., Omura, Y., et al., 2010. Cluster observations of emic triggered emissions in association with pc1 waves near earth's plasmapause. Geophys. Res. Lett. 37 (9). https://doi.org/10.1029/2010GL042648.

Remya, B., Sibeck, D., Halford, A., et al., 2018. Ion injection triggered emic waves in the earth's magnetosphere. J. Geophys. Res.: Space Phys. 123 (6), 4921–4938. https://doi.org/10.1029/2018JA025354.

Remya, B., Tsurutani, B., Reddy, R., et al., 2015. Electromagnetic cyclotron waves in the dayside subsolar outer magnetosphere generated by enhanced solar wind pressure: Emic wave coherency. J. Geophys. Res.: Space Phys. 120 (9), 7536–7551. https://doi.org/10.1002/2015JA021327.

Saikin, A., Zhang, J.-C., Allen, R., et al., 2015. The occurrence and wave properties of h^+, he^+, and o^+ band emic waves observed by the van allen probes. J. Geophys. Res.: Space Phys. 120 (9), 7477–7492. https://doi.org/10.1002/2015JA021358.

Sakaguchi, K., Kasahara, Y., Shoji, M., et al., 2013. Akebono observations of emic waves in the slot region of the radiation belts. Geophys. Res. Lett. 40 (21), 5587–5591. https://doi.org/10.1002/2013GL058258.

Shprits, Y.Y., Kellerman, A., Aseev, N., et al., 2017. Multi-mev electron loss in the heart of the radiation belts. Geophys. Res. Lett. 44 (3), 1204–1209. https://doi.org/10.1002/2016GL072258.

Shreedevi, P.R., Yu, Y., Ni, B., et al., 2021. Simulating the ion precipitation from the inner magnetosphere by h-band and he-band electro magnetic ion cyclotron waves. J. Geophys. Res.: Space Phys. 126 (3). https://doi.org/10.1029/2020JA028553, e2020JA028553.

Tetrick, S.S., Engebretson, M.J., Posch, J.L., et al., 2017. Location of intense electromagnetic ion cyclotron (emic) wave events relative to the plasmapause: Van allen probes observations. J. Geophys. Res.: Space Phys. 122 (4), 4064–4088. https://doi.org/10.1002/2016JA023392.

Thorne, R.M., Horne, R.B., 1994. Energy transfer between energetic ring current h+ and o+ by electromagnetic ion cyclotron waves. J. Geophys. Res.: Space Phys. 99 (A9), 17275–17282. https://doi.org/10.1029/94JA01007.

Thorne, R.M., Horne, R.B., 1997. Modulation of electromagnetic ion cyclotron instability due to interaction with ring current o+ during magnetic storms. J. Geophys. Res.: Space Phys. 102 (A7), 14155–14163. https://doi.org/10.1029/96JA04019.

Turner, D., Morley, S., Miyoshi, Y., et al., 2012. Outer radiation belt flux dropouts: Current understanding and unresolved questions. Dyn. Earth's Radiat. Belts Inner Magnetosphere 199, 195–212. https://doi.org/10.1029/2012GM001310.

Turner, D.L., Ukhorskiy, A.Y., 2020. Outer radiation belt losses by magnetopause incursions and outward radial transport: New insight and outstanding questions from the van allen probes era. In: The Dynamic Loss of Earth's Radiation Belts. Elsevier, pp. 1–28. https://doi.org/10.1016/B978-0-12-813371-2.00001-9.

Upadhyay, A., Kakad, B., Kakad, A., et al., 2020. Occurrence characteristics of electromagnetic ion cyclotron waves at sub-auroral antarctic station maitri during solar cycle 24. Earth, Planets Space 72 (1), 1–16. https://doi.org/10.1186/s40623-020-01157-7.

Upadhyay, A., Kakad, B., Kakad, A., et al., 2022a. Effect of solar wind pressure and substorm linked particle injection on local time distribution of electromagnetic ion cyclotron waves. Front. Astron. Space Sci. 9, 866023. https://doi.org/10.3389/fspas.2022.866023.

Upadhyay, A., Kakad, B., Kakad, A., Rawat, R., 2022b. A Statistical Study of Modulation of Electromagnetic Ion Cyclotron Waves Observed on Ground. J. Geophys. Res.: Space Phys. 127. https://doi.org/10.1029/2022JA030340 e2022JA030340.

Usanova, M., Drozdov, A., Orlova, K., et al., 2014. Effect of emic waves on relativistic and ultrarelativistic electron populations: Ground-based and van allen probes observations. Geophys. Res. Lett. 41 (5), 1375–1381. https://doi.org/10.1002/2013GL059024.

Usanova, M., Mann, I., Rae, I., et al., 2008. Multipoint observations of magnetospheric compression-related emic pc1 waves by themis and carisma. Geophys. Res. Lett. 35 (17). https://doi.org/10.1029/2008GL034458.

Usanova, M.E., Darrouzet, F., Mann, I.R., et al., 2013. Statistical analysis of emic waves in plasmaspheric plumes from cluster observations. J. Geophys. Res.: Space Phys. 118 (8), 4946–4951. https://doi.org/10.1002/jgra.50464.

Vines, S., Allen, R., Anderson, B., et al., 2019. Emic waves in the outer magnetosphere: Observations of an off-equator source region. Geophys. Res. Lett. 46 (11), 5707–5716. https://doi.org/10.1029/2019GL082152.

Wang, H., He, Y., Lühr, H., et al., 2019. Storm time emic waves observed by swarm and van allen probe satellites. J. Geophys. Res.: Space Phys. 124 (1), 293–312. https://doi.org/10.1029/2018JA026299.

Wang, H., He, Y.F., Lühr, H., et al., 2021. Local time and longitudinal differences in the occurrence frequency of ionospheric emic waves during magnetic storm periods. J. Geophys. Res.: Space Phys. 126 (2). https://doi.org/10.1029/2020JA028878, e2020JA028878.

Xiang, Z., Tu, W., Li, X., et al., 2017. Understanding the mechanisms of radiation belt dropouts observed by van allen probes. J. Geophys. Res.: Space Phys. 122 (10), 9858–9879. https://doi.org/10.1002/2017JA024487.

Yahnin, A.G., Popova, T.A., Demekhov, A.G., et al., 2021. Evening side emic waves and related proton precipitation induced by a substorm. J. Geophys. Res.: Space Phys. n/a(n/a). https://doi.org/10.1029/2020JA029091, e2020JA029091.

Yuan, Z., Liu, K., Yu, X., et al., 2018. Precipitation of radiation belt electrons by emic waves with conjugated observations of noaa and van allen satellites. Geophys. Res. Lett. 45 (23), 12694–12702. https://doi.org/10.1029/2018GL080481.

Zhang, J.-C., Saikin, A., Kistler, L.M., et al., 2014. Excitation of emic waves detected by the van allen probes on 28 April 2013. Geophys. Res. Lett. 41 (12), 4101–4108. https://doi.org/10.1002/2014GL060621.